



Reusable UiO-66-NH₂ Functionalized Polyacrylonitrile Nanofiber Membrane for Effective Removal of Cr(VI) from Water

Bing Deng Wang¹ · Bismark Sarkodie¹ · Xu Yang¹ · Yun Tao¹ · Ze Mao¹ · Ling Ling Zhao¹ · Quan Feng¹

Received: 27 July 2023 / Revised: 9 November 2023 / Accepted: 3 December 2023 / Published online: 13 February 2024
© The Author(s), under exclusive licence to the Korean Fiber Society 2024

Abstract

Metal–organic framework UiO-66-NH₂ powder used for effective removal of Cr(VI) from water is difficult to recover after usage. In this study, UiO-66-NH₂ was in-situ grown on polyacrylonitrile (PAN) nanofiber membrane using water as solvent and trifluoroacetic acid as structure regulator, via hydrothermal method for adsorption of Cr(VI) ions. The optimal proportion of trifluoroacetic acid, hydrothermal synthesis time and pH level were 30%, 4 h and pH = 2, respectively. Scanning electron microscopy showed that UiO-66-NH₂ was uniformly and densely coated on the PAN nanofibers. N₂ adsorption–desorption experiments and thermogravimetric analysis showed large surface area (680.99 m²/g) and good thermal stability of PAN@UiO-66-NH₂ compared to PAN nanofiber membrane. The adsorption capacity of PAN@UiO-66-NH₂ nanofiber membrane for Cr(VI) at 298 K was 312.25 mg/g. Kinetic studies revealed that the adsorption process was consistent with Langmuir isotherm and pseudo-second-order model. The composite showed good reusability in Cr(VI) removal in 5 cycles. Based on Zeta potential, the influence of pH and XPS analysis, PAN@UiO-66-NH₂ nanofiber membrane effectively adsorbs Cr(VI) through electrostatic interaction. PAN@UiO-66-NH₂ nanofiber membrane is therefore considered as an efficient and reusable adsorbent with high potential for Cr(VI) removal in industrial wastewater.

Keywords Adsorption · Electrospinning · Metal–organic framework · Cr(VI) ions · Polyacrylonitrile nanofibers

1 Introduction

With the development in mining, smelting, battery and leather manufacturing industries, heavy metals such as chromium, nickel, lead, cadmium, copper, etc. are seriously polluting water, and the treatment of industrial wastewater is also becoming more challenging [1, 2]. Among these heavy metal pollutants, Cr(VI) is a non-degradable heavy metal identified as the most teratogenic, carcinogenic and highly toxic. The removal of Cr(VI) heavy metal pollutant from wastewater is very challenging [3]. Therefore, it has been imperative to develop efficient treatment technologies to remove Cr(VI) from wastewater. Although many technological strategies such as electrocoagulation [4], catalytic reduction [5], membrane systems [6] and photocatalysis [7], adsorption technology is still more favored due to its

flexibility, economical, effective and simplistic attributes. This makes it necessary to design and explore a low-cost and reusable adsorbent with efficient adsorption capacity.

In the past few decades, researchers have proposed metal organic framework (MOFs) materials as a new type of porous adsorbent. Comparatively, most MOFs have large surface area and porosity, much higher than popularly used carbon and zeolite materials [8]. MOFs such as UiO-66 is finding wider application in environmental remediation. The UiO-66 is composed of [Zr₆O₄(OH)₄] metal clusters and 12 terephthalic acid (H₂BDC) complexes, with the highest organic ligand and metal cluster [9]. The UiO-66 is easy to modify since ideal physical and chemical properties can be obtained by modifying its functional groups [10]. By coordinating other functional groups on the ligand with Zr, functionalized Zr MOFs can be prepared, such as UiO-66-NH₂, UiO-66-NO₂, etc. [11]. Wang et al. [12] reveal that the modification of UiO-66-NH₂ with phenothiazine-N-rhodanine improves the removal of Cr(VI), with maximum absorption capacity of 333.67 mg/g at 303 K and pH = 2, better than unmodified UiO-66-NH₂. Wang et al. [13] report maximum adsorption capacity of Cr(VI) at 243.9 mg/g on

✉ Quan Feng
fengquan@ahpu.edu.cn

¹ Advanced Fiber Materials Engineering Research Center of Anhui Province, Anhui Polytechnic University, Wuhu 241000, Anhui, China

formic acid-modified-UiO-66, which were extremely better than unmodified UiO-66 (36.4 mg/g). This reveals that the modification or synthesis conditions of the MOF adsorbent has a significant influence on the performance of the adsorbent. Although UiO-66-NH₂ particles are effective in wastewater treatment, recycling or reusability has been time-demanding, complex and a huge challenge. The UiO-66-NH₂ particles also tend to agglomerate during application, which affects the exposure of active sites and the performance of the adsorbent. Therefore, keen interest has been on the engineering of efficient UiO-66-NH₂ adsorbent that can be easily recycled and reused. Zhang et al. [14] report efficient catalyzation of 2-chloroethyl ethyl sulfide using TFA-modulated-UiO-66-NH@polyacrylonitrile (PAN) nanofiber membrane. San et al. [15] developed UiO-66-NH₂ and electrospun with PAN/chitosan to obtain membrane which was effective in removing heavy metal ions from water. However, the presence of already synthesized solid-UiO-66-NH₂ could easily agglomerate and affect the dispersion of UiO-66-NH₂ in the composite. Also, surface-coverage of active MOFs with the polymer is inevitable in this strategy. At present, effective methods for loading surface-active MOFs onto nanofibers include spray coating method [16], blending method [17], in-situ growth method [18], etc. In-situ growth method is a one pot synthesis method that combines substrate materials, metal salts, and organic ligands, as polymer substrates, MOFs precursors, and metal salts can be directly added to the solvent to develop into oxide from the atomic level to create strong bond with the surface of the substrate. In other words, the growth of MOFs on the surface rather than inside the polymer during synthesis can avoid the common challenge of MOFs agglomeration.

In this study, a reusable UiO-66-NH₂ adsorbent was prepared by a simple in-situ growth of UiO-66-NH₂ (using water as solvent) on electrospun PAN nanofiber membrane (PAN nanofiber membrane has uniform thickness and layered structures between fibers, which can serve as a good substrate for the growth of UiO-66-NH₂), with Trifluoroacetic acid (TFA) as the regulator during synthesis. Various samples were characterized and the effect of varying TFA concentration, hydrothermal synthesis time and pH, Cr(VI) concentrations, interference ions in wastewater on adsorption capacity were systematically examined. Furthermore, the adsorption mechanism was analyzed by fitting the experimental data of adsorption kinetics and isotherm.

2 Experimental Section

2.1 Materials

2-Aminoterephthalic acid (NH₂-H₂BDC), zirconium chloride (ZrCl₄), Trifluoroacetic acid (TFA), *N,N*-dimethylformamide

(DMF), FeCl₃·6H₂O, CaCl₂, ZnSO₄·7H₂O, anhydrous ethanol were purchased from Shanghai Maclean Biochemical Technology Co., Ltd; Potassium dichromate (K₂Cr₂O₇) was purchased from Tianjin Chemical Reagent Research Institute; Acetone, concentrated hydrochloric acid, concentrated sulfuric acid were purchased from Tianjin Beilian Fine chemical Development Co., Ltd; Polyacrylonitrile (PAN *M_w* = 90,000), KCl, purchased from Sinopharm Reagent Network. Other reagents, such as PbCl₂, CuCl₂, ZnCl₂, CdCl₂, and NiCl₂·6H₂O were purchased from Shanghai Aladdin Biochemical Technology Co., Ltd; Zn(NO₃)₂·6H₂O was purchased from Xilong Chemical Co., Ltd. Electrospinning machine (HZ-14 Electrospinning machine Qingdao Nuokang Environmental Protection Technology Co., Ltd.) was used to prepare nanofiber membrane. The materials and reagents were analytical grade and used without further purification.

2.2 Characterization

Scanning electron microscope (SEM, Hitachi S-4800 Scanning electron microscope) was used to observe the surface morphology of the samples. The samples were coated with gold before observation. X-ray diffractometer (XRD, Germany Bruker D8 Advance) was used to analyze the crystal structure of the samples (the scanning range was set at 5°–60°). The composition and structure of the sample were analyzed using a Fourier transform infrared spectrometer (FTIR, IR Prestige-21 model from Shimadzu Corporation, Japan), with a wavelength range of 4000–500 cm⁻¹. The thermal stability of sample was tested with a thermogravimetric differential thermal analyzer (TG, American TA TGA 550). The temperature test range was from 30 to 800 °C, and the heating ramp rate was 10 °C/min. The specific surface area, pore size distribution, and pore volume of thin film samples were tested using a fully automated surface area and porosity analyzer (BET, Micromeritics ASAP 2460, USA). Nitrogen gas was used and the degassing temperature was 120 °C. An X-ray photoelectron spectroscopy (XPS, Thermo Scientific K-Alpha, USA) was used to analyze the chemical element valence states of samples.

2.3 Preparation of PAN Nanofiber Membrane

An amount of PAN powder (3 g) was weighed and dissolve in 27 g DMF, stir for 6 h, to obtain a uniform and bubble-free PAN spinning solution. The solution was then poured into the syringe attached with 20-gauge needle. The electrospinning parameter used include: 18 kV, solution flow rate of 0.8 mL/h and the rotating speed of cylindrical drum collector was 140 r/min. The distance between the tip of the needle and the collector was 20 cm. After spinning, the PAN nanofiber membrane was removed and dried at 60 °C overnight.

2.4 Preparation of PAN@UiO-66-NH₂ Nanofiber Membranes Using Different TFA Contents

In this step, 5 bottles of solvents with different TFA contents: 10, 20, 30, 40, and 50% were setup (the total volume of deionized water and TFA was 30 mL in each bottle). An amount of 349.56 mg of ZrCl₄ (1.5 mmol) and 407.57 mg of NH₂-H₂BDC (2.25 mmol) were accurately weighed and added to the five bottled dilute TFA solvent, and sonicated for 30 min. PAN nanofiber membranes (5 cm × 5 cm each) were immersed in the above-mentioned 5 different solutions and sonicated. The mixtures were then poured into autoclave for hydrothermal reaction at 100 °C for 4 h. The samples were washed with deionized water, and then dried at 60 °C for later use. For subsequent experimental work, PAN@UiO-66-NH₂ prepared with 30% TFA (30%-PAN@UiO-66-NH₂) since UiO-66-NH₂ was well-grown on its surface.

2.5 Preparation of PAN@UiO-66-NH₂ Nanofiber Membranes at Different Hydrothermal Time

Firstly, 4 bottles of solvent with a 30% TFA content (30 mL) were setup. An amount of 349.56 mg of ZrCl₄ and 407.57 mg of NH₂-H₂BDC were added into each solvent and sonicated for 30 min. PAN nanofiber membranes (5 cm × 5 cm each) were placed in the precursor mixture and poured into autoclaves for hydrothermal reaction at 100 °C for 1, 2, 4, and 6 h. After the set time, the samples were washed with deionized water, and then dried overnight in an oven at 60 °C. The specific preparation method is shown in Fig. 1.

2.6 Adsorption Experiment

Using single variable method, the impact of different factors (concentration of TFA (%), pH, hydrothermal synthesis time, etc.) on PAN@UiO-66-NH₂ nanofiber membrane

for the adsorption of Cr(VI) was assessed. The adsorption kinetics, isotherm and reusability of samples are also discussed. During the adsorption experiment, the PAN@UiO-66-NH₂ nanofiber membrane (20 mg) was added to a certain concentration of Cr(VI) solution (20 mL; concentration of 100 mg/L). The solution was oscillated in a constant temperature (308 K) at 120 rpm for 24 h. The Cr(VI) removal efficiency from the solution was tested with UV spectrophotometer (SHIMADZU UVmini 1285) at 540 nm to detect the residual Cr(VI) concentration after equilibrium adsorption. Equations (1) and (2) were used to calculate the adsorption amount Q_e (mg/g) and removal rate R :

$$Q_e = \frac{(C_0 - C_e)V}{m} \quad (1)$$

$$R = \frac{C_0 - C_e}{C_0} \times 100\% \quad (2)$$

In the formula, Q_e is the adsorption capacity of Cr(VI) in mg/g; R is the removal rate of Cr(VI) (%); V is the volume of Cr(VI) solution (mL); m is the mass of the adsorbent (g); C_0 and C_e are the mass concentrations (g/L) of Cr(VI) at the initial and equilibrium times.

2.7 Effect of pH on Adsorption Performance

Similar experimental conditions in Sect. 2.6. were used in assessing the effect of pH on adsorption performance of 30%-PAN@UiO-66-NH₂. The pH of the solution was adjusted with 0.1 mol/L NaOH and 0.1 mol/L HCl from the range of pH = 1 to pH = 12, at 308 K for 24 h. The concentration of Cr(VI) in the solution was examined with UV spectrophotometer and the adsorption efficiency was calculated using Eqs. (1) and (2).

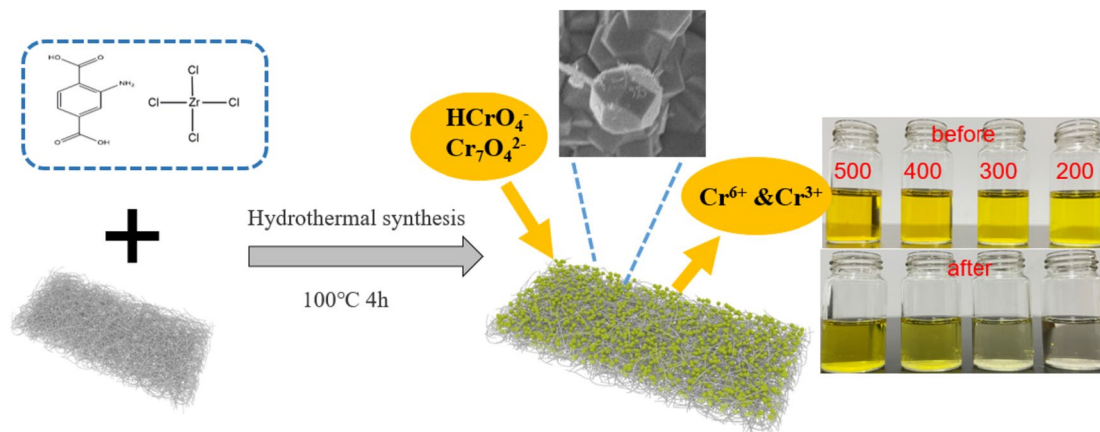


Fig. 1 Schematic representation of PAN@UiO-66-NH₂ preparation and the removal process

2.8 Effect of Cr(VI) Concentration on Adsorption Performance

Similar experimental conditions in Sect. 2.6 were used in assessing the effect of Cr(VI) concentration on adsorption performance of 30%-PAN@UiO-66-NH₂. The assessment was done in initial Cr(VI) solution concentrations of 50–500 mg/L in pH 2 (best pH environment with highest adsorption capacity) at 308 K for 24 h. Finally, the concentration of Cr(VI) in the solution was examined with UV spectrophotometer and the adsorption efficiency was calculated using Eqs. (1) and (2).

2.9 Adsorption Kinetics Study

Similar experimental conditions in Sect. 2.8 were used in assessing the effect of Cr(VI) concentration on adsorption performance of 30%-PAN@UiO-66-NH₂ at 308 K and 120 rpm. The analysis with UV spectrophotometer was done at regular interval to determine the removal efficiency of Cr(VI) in water. The linear Eqs. (3) and (4) are shown below:

$$\ln(Q_e - Q_t) = \ln Q_e - K_1 t \quad (3)$$

$$\frac{t}{Q_t} = \frac{1}{K_2 Q_e^2} + \frac{t}{Q_e} \quad (4)$$

In the formula, Q_e is the adsorption capacity when the adsorption reaches equilibrium (mg/g); Q_t is the adsorption capacity with respect to time t (mg/g); K_1 is the reaction rate constant of the pseudo first-order model (min⁻¹); K_2 is the reaction rate constant of the pseudo second order model (min⁻¹g/mg).

2.9.1 Assessment of Adsorption Isotherm

PAN@UiO-66-NH₂ nanofiber membranes (20 mg) were placed in solutions with an initial Cr(VI) concentration of 50–500 mg/L at different temperatures (298, 308, and 318 K), pH=2, and constant shaking speed of 120 rpm for 24 h. The adsorption isotherms were fitted to the experimental adsorption data by Langmuir model Eq. (5) and Freundlich model Eq. (6).

$$\frac{1}{Q_e} = \frac{1}{Q_m} + \frac{1}{Q_m K_L C_e} \quad (5)$$

$$\ln Q_e = \ln K_F + \frac{1}{n} \ln C_e \quad (6)$$

In the formula, Q_e is the adsorption amount at adsorption equilibrium (mg/g); Q_m is the maximum adsorption

capacity (mg/g); C_e is the concentration of the solution at adsorption equilibrium (mg/L); K_L is the Langmuir model constant (L/g); K_F is the Freundlich adsorption constant; n is the Freundlich constant.

2.9.2 Effect of Interference Ions on Adsorption Performance

An amount of 10 mL cationic solutions (K⁺, Ni²⁺, Cd²⁺, Ca²⁺, Zn²⁺, Fe³⁺, Pb²⁺, Cu²⁺, all at a concentration of 100 mg/L) and 10 mL anionic solutions (Cl⁻, NO₃⁻, SO₄²⁻, with a concentration range of 5–20 mmol/L) were added to 10 mL Cr(VI) solution. PAN@UiO-66-NH₂ nanofiber membrane (10 mg) was immersed in the above solutions, controlled at pH=2 and 308 K for 24 h. Similarly, 10 mL anionic solutions (Cl⁻, NO₃⁻, SO₄²⁻) with a concentration range of 5–20 mmol/L were added to 10 mL Cr(VI) solution. The average of the results was deduced from three repeated experimental tests and used to calculate the removal rate and adsorption amount of Cr(VI) ions.

2.9.3 Reusability Test

PAN@UiO-66-NH₂ nanofiber membrane (20 mg) was immersed in 100 mg/L Cr(VI) solution, controlled at pH=2 and 308 K for 24 h. After the end of each adsorption cycle, the PAN@UiO-66-NH₂ nanofiber membrane was immersed in sodium hydroxide solution (pH=12), stirred gently for 1 h, washed with deionized water to neutral, and then subjected to the adsorption test again after drying. This test was repeated five times to provide solid information about the reusability of the sample. In general, three samples were setup for each cycle and their average values were taken.

3 Results and Discussion

3.1 XRD Analysis

Figure 2 shows the XRD patterns of PAN@UiO-66-NH₂ samples synthesized with different percentage of Trifluoroacetic acid (TFA). The PAN@UiO-66-NH₂ synthesized with 10, 20, 30, 40 and 50% TFA are denoted as 10%-PAN@UiO-66-NH₂, 20%-PAN@UiO-66-NH₂, 30%-PAN@UiO-66-NH₂, 40%-PAN@UiO-66-NH₂, and 50%-PAN@UiO-66-NH₂, respectively. Characteristic diffraction peaks located at 7.4° and 8.5°, corresponding to the (111) and (002) crystal planes of UiO-66-NH₂, respectively, consistent with literature reports [19]. The peaks around 5.3° could be assigned to missing cluster defect which could aid in the formation of an eight-connected reotopology [14]. A very broad peak in a range of 10°–20° corresponds to the low crystallinity of PAN [20]. Comparatively, the 20%-PAN@

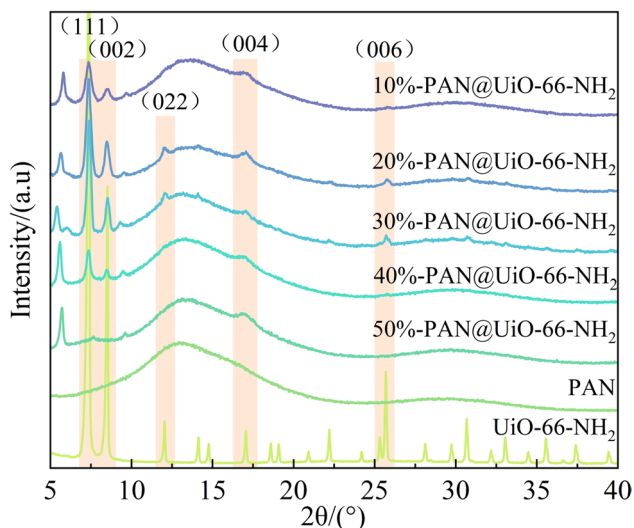


Fig. 2 XRD patterns of PAN@UiO-66-NH₂ nanofibrous membrane synthesized using different contents of TFA, PAN and UiO-66-NH₂

UiO-66-NH₂ and 30%-PAN@UiO-66-NH₂ show sharp diffraction peaks at 7.4° and 8.5°, indicating the existence of highly crystalline UiO-66-NH₂ on PAN@UiO-66-NH₂ prepared in the presence of 20 and 30% TFA. At a concentration of 10 and 40% TFA, weak peaks appeared at 7.4° and 8.5°. There was no significant peak of UiO-66-NH₂ identified on PAN@UiO-66-NH₂ synthesized in 50% TFA, implying an unsuccessful synthesis of UiO-66-NH₂ on PAN in 50% TFA concentration.

3.2 SEM Analysis

Figure 3a–h shows the SEM images of PAN nanofiber membrane, UiO-66-NH₂ and PAN@UiO-66-NH₂ prepared with different TFA content. No obvious regular crystal shape of UiO-66-NH₂ was observed on 10%-PAN@UiO-66-NH₂, but thin layers of UiO-66-NH₂ with ~0.5 μm size were grown on the surface of PAN nanofiber membrane in 20%-PAN@UiO-66-NH₂. On the other hand, regular crystals of UiO-66-NH₂ grew on PAN nanofiber membrane in the shape of "beads", with a size of about 2–2.5 μm on 30%-PAN@

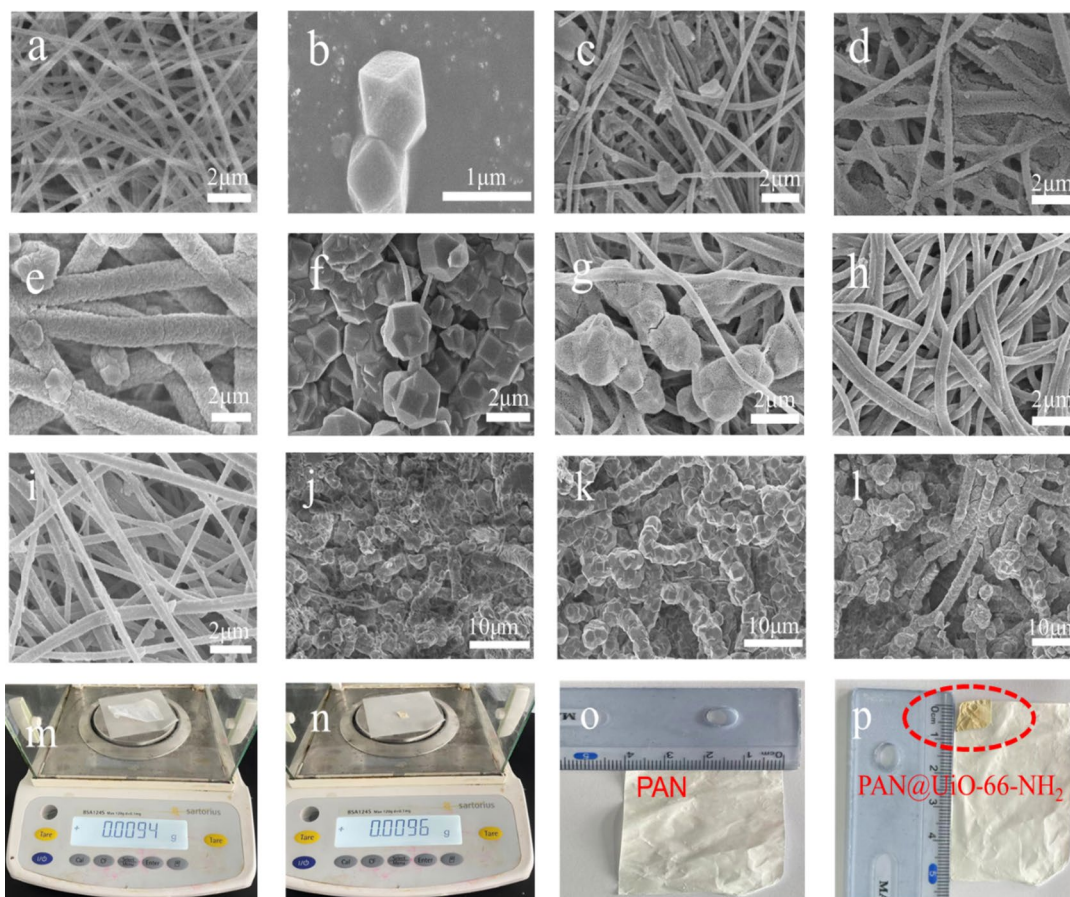


Fig. 3 SEM images of PAN@UiO-66-NH₂ nanofibrous membrane synthesized using different contents of TFA: **a** PAN, **b** UiO-66-NH₂, **c** 0%, **d** 10%, **e** 20%, **f** 30%, **g** 40% and **h** 50%. SEM images of 30%-

PAN@UiO-66-NH₂ nanofibrous membrane synthesized by different hydrothermal growth time: **i** 1 h, **j** 2 h, **k** 4 h and **l** 6 h. **m–p** Physical drawing of PAN and PAN@UiO-66-NH₂ nanofibrous membrane

UiO-66-NH₂. However, the increase in the concentration of TFA to 40% negatively affected the growth of UiO-66-NH₂ in 40%-PAN@UiO-66-NH₂, resulting in no well-defined UiO-66-NH₂ crystal formation. Furthermore, smooth surface of PAN nanofibers was observed on 50%-PAN@UiO-66-NH₂. This indicates that there is no significant and distinguishable UiO-66-NH₂ formed on the surface of PAN nanofibers when the concentration of TFA was increased to 50%. It is worth noting that the difference in morphological structure and growth of UiO-66-NH₂ in the various samples can be primarily assigned to the acidity of TFA solution. Trifluoroacetic acid, as a regulator, can adjust the acidity of solvent prominently as the concentration of TFA increases. It has been propounded that the higher acidity of TFA slowed down the crystallization to yield a continuous coating, so that zirconium ions can better combine with PAN nanofiber membrane. This preferentially enhances the growth of UiO-66-NH₂ on the nanofiber membrane, especially at 30%-PAN@UiO-66-NH₂, rather than depositing UiO-66-NH₂ in the solvent [21]. However, the higher concentration of Trifluoroacetic acid in 40%-PAN@UiO-66-NH₂, and 50%-PAN@UiO-66-NH₂ tends to exorbitantly slow down the growth of UiO-66-NH₂ on the PAN nanofibers; hence, the loading rate of UiO-66-NH₂ on the PAN nanofiber membrane was significantly decreased [22]. The trend in SEM image analysis of the samples is consistent with the XRD results discussed previously. Given that the XRD and SEM results reveal that 30%-PAN@UiO-66-NH₂ had well-grown and developed UiO-66-NH₂ on the surface of PAN nanofiber membrane, it was chosen for further experimental studies and analysis.

3.3 Effect of Hydrothermal Reaction Time on UiO-66-NH₂ Growth

Figure 3i–j show the images of 30%-PAN@UiO-66-NH₂ fabricated in different hydrothermal reaction time. As shown in the figure, smooth surface of PAN nanofiber membrane

was observed when hydrothermal reaction was done in 1 h. This implies that UiO-66-NH₂ cannot be formed within that stipulated time. On the other hand, UiO-66-NH₂ grew on the PAN nanofiber membrane when 2 h hydrothermal time was employed. Regular UiO-66-NH₂ particles successfully grew on PAN nanofiber membrane in the form of "beads" at 4 h reaction time. Similar to the image of sample prepared in 2 h, a dense and undefined layer of UiO-66-NH₂ particles were grown on the surface of PAN nanofiber membrane when the hydrothermal reaction time was increased to 6 h. This implies that well-grown and good surface coverage of regular bead-like UiO-66-NH₂ particles are successfully formed in 4 h hydrothermal synthesis time.

3.4 Specific Surface Area and Pore Volume Analysis

Figure 4a, b shows the N₂ adsorption-desorption curve and pore size distribution of nanofiber membranes. The textural properties of samples are tabulated in Table 1. The PAN nanofiber membrane recorded a surface area, pore volume and average pore size of 9.94 m²/g, 0.026 cm³/g and 15.32 nm, respectively. After growing UiO-66-NH₂ on PAN

Table 1 Surface area and pore size of PAN and PAN@UiO-66-NH₂ nanofiber membranes

Samples	Specific surface area (m ² /g)	Pore volume (cm ³ /g)	Pore size (nm)
PAN nanofiber membrane	9.94	0.026	15.32
UiO-66-NH ₂	847.53	0.383	4.46
30%2h-PAN@UiO-66-NH ₂	536.72	0.256	4.62
30%4h-PAN@UiO-66-NH ₂	680.99	0.333	3.99
30%6h-PAN@UiO-66-NH ₂	621.84	0.298	4.43

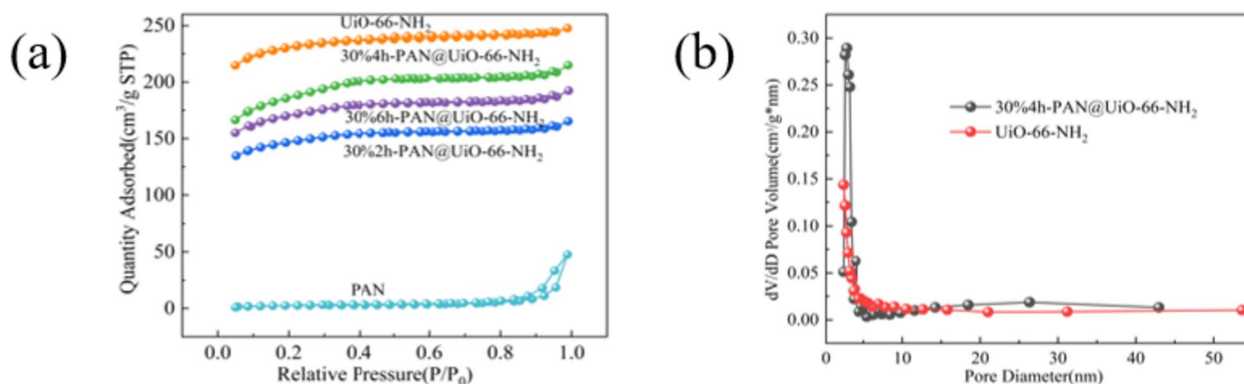


Fig. 4 a N₂ adsorption–desorption curve and b pore size distribution of PAN, UiO-66-NH₂ and PAN@UiO-66-NH₂ nanofiber membranes

nanofiber membranes, the textural properties of nanofiber membranes significantly improved. This is primarily related to the impact of large surface area UiO-66-NH₂ particles grown on the surface of PAN nanofiber membranes. Among all the PAN@UiO-66-NH₂ samples, 30%-PAN@UiO-66-NH₂ synthesized for 4 h (30%4h-PAN@UiO-66-NH₂) displays the largest surface area and pore volume, which is a prospect for improvement in adsorption pollutants. Compared to PAN nanofiber membrane, the surface area and pore volume of 30%4h-PAN@UiO-66-NH₂ increased by ~68.5 times and ~12.8 times, respectively, which is conducive to enhance adsorption. Considering time, energy, cost, surface area and the successful growth of UiO-66-NH₂ particles on PAN nanofiber membranes observed in XRD and SEM results, 30%4h-PAN@UiO-66-NH₂ was used for subsequent experiments.

3.5 FTIR Analysis

Figure 5a shows the FTIR spectra of PAN and 30%4h-PAN@UiO-66-NH₂ nanofiber membranes. The characteristic peak of PAN at 2235 cm⁻¹ is attributed to the vibration of C≡N in PAN nanofibers [23]. After successfully loading of UiO-66-NH₂ on PAN (30%4h-PAN@UiO-66-NH₂), new absorption peaks at 1420, 1205, 765, and 661 cm⁻¹ appeared. The new adsorption peak at 1420 cm⁻¹ is attributed to the bending vibration of C–O [24]; the peak at 1205 cm⁻¹ corresponds to the characteristic peak of C_{ar}–N [25]; and the peaks at 765 and 661 cm⁻¹ are attributed to the stretching vibration of Zr–O [26]. Based on the above results, it could be further confirmed that PAN@UiO-66-NH₂ was successfully synthesized.

3.6 TGA Analysis

To explore the thermal stability of PAN@UiO-66-NH₂, thermogravimetric analysis test was carried out. As shown

in Fig. 5b, 30%4h-PAN@UiO-66-NH₂ recorded a weight loss before 280 °C, relating to the dehydration and dehydroxylation of MOFs structure [14]. The weight loss between 280 and 800 °C is attributed to the decomposition of NH₂-H₂BDC organic ligands, causing the crystal structure of UiO-66-NH₂ to be destroyed, resulting in complete collapse of their structure. Simultaneously, PAN nanofiber membrane undergoes pyrolysis [27]. No significant mass loss was observed after 520 °C. The enhanced stability of 30%4h-PAN@UiO-66-NH₂ even after 280 °C compared to PAN (decomposition temperature = ~260 °C) [28] indicates good thermal stability, resulting from the growth of UiO-66-NH₂ particles on the surface of PAN nanofiber membranes.

3.7 Effect of pH on Adsorption and Zero-Point Analysis

The adsorption results of Cr(VI) on 30%4h-PAN@UiO-66-NH₂ nanofiber membranes at different pH values and the surface charge during adsorption test was obtained and illustrated in Fig. 6. Based on the results presented in Fig. 6a, it could be stated that pH does not only affect the adsorption capacity of the adsorbent, but also affects the surface charge of chromium ions. The experimental results indicate that the adsorption capacity of 30%4h-PAN@UiO-66-NH₂ decreases as the pH value increases above 2 (Fig. 6a). At pH = 12, almost zero adsorption capacity was recorded. This implies that under alkaline condition, the adsorption capacity is significantly affected. At pH 2–6, chromium ions mainly exist in the form of HCrO₄⁻ and Cr₂O₇²⁻. When the pH exceeds 6, chromium ions exist in the form of CrO₄²⁻ [29]. The experimental results in Fig. 6a show that when the pH increases from 1 to 13.5, the zeta potential shows an increase in surface charge from ~25 mV at pH = 1 to ~27 mV at pH = 2 and a sudden decrease in surface charge after pH = 2. Furthermore, when pH level is

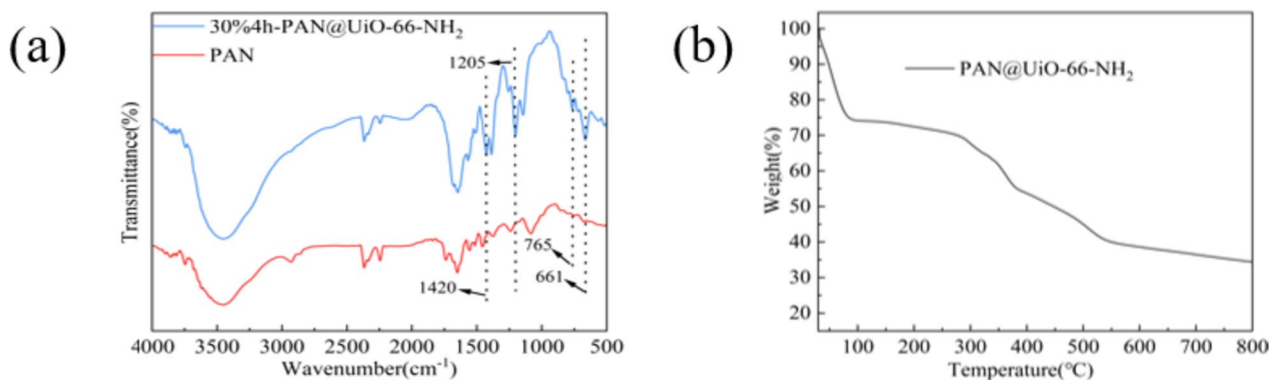


Fig. 5 **a** FT-IR spectra of PAN and 30%4h-PAN@UiO-66-NH₂ nanofiber membranes. **b** Thermogravimetry curves of 30%4h-PAN@UiO-66-NH₂ nanofiber membrane

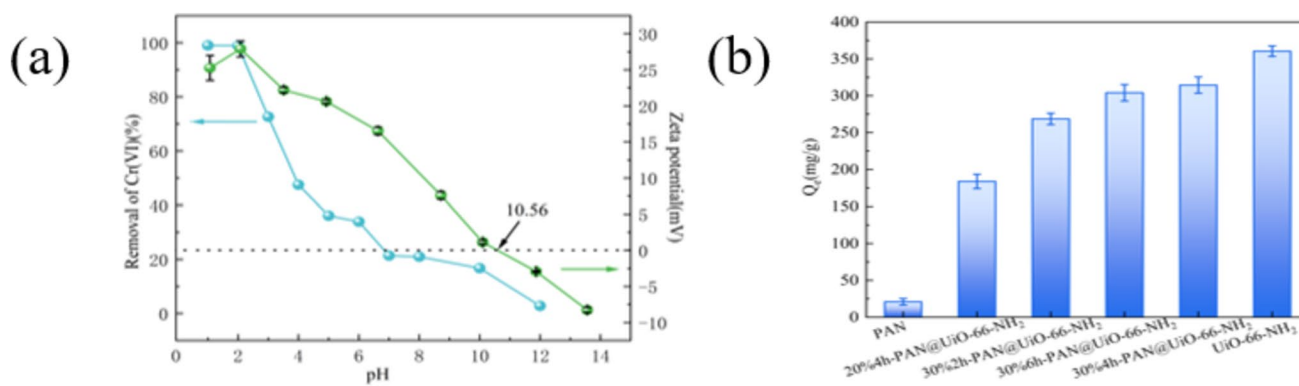


Fig. 6 a Cr(VI) removal rates on 30%4h-PAN@UiO-66-NH₂ nanofiber membranes at different pH levels and Zeta potentials at different pH and b effect of trifluoroacetic acid concentration and synthesis time on adsorption capacity

having more than zero zeta potential (lower pH level), H⁺ in water combines with NH²⁺ groups on the surface of UiO-66-NH₂, deprotonates and forms NH³⁺ groups. This implies that the 30%4h-PAN@UiO-66-NH₂ carries a positive charge on its surface, which is beneficial for electrostatic attraction of anionic pollutants [30]. When the pH level has less than zero zeta potential (higher pH level), 30%4h-PAN@UiO-66-NH₂ exhibits high negative charges on its surface, which generates electrostatic repulsion towards anionic pollutants and reduce adsorption efficiency. Since pH = 2 has the highest positive net charge and best performance under different pH, subsequent adsorption experiments were conducted under the condition of pH = 2.

Figure 6b shows the adsorption performance of PAN@UiO-66-NH₂ prepared with different TFA concentration and synthesis time at pH = 2. To elucidate the efficiency of the samples, UiO-66-NH₂ particles and 20%4 h-PAN@UiO-66-NH₂ (that is, 20%-PAN@UiO-66-NH₂ synthesized for 4 h) were used as reference. Pristine UiO-66-NH₂ (solely particles) has the highest adsorption capacity, reaching 360.55 mg/g, while the lowest adsorption capacity was recorded on PAN nanofiber membrane (20.9 mg/g). The synthesis of PAN@UiO-66-NH₂ composites had significant improvement in the adsorption capacity of PAN nanofiber membrane. Among the PAN@UiO-66-NH₂ samples, 30%4h-PAN@UiO-66-NH₂ and 30%6h-PAN@UiO-66-NH₂ recorded the highest adsorption capacity of 312.25 and 314.47 mg/g, respectively. This implies that there is an insignificant improvement in the adsorption capacity of PAN@UiO-66-NH₂ composites after 4 h hydrothermal synthesis time. The relatively lower capacity of reusable 30%4h-PAN@UiO-66-NH₂ and 30%6h-PAN@UiO-66-NH₂ compared to pure UiO-66-NH₂ particles is due to unequal load of UiO-66-NH₂ in these two samples (lower % of UiO-66-NH₂ is loaded on the PAN nanofiber membrane in hydrothermal method; the 20 mg sample used for the test includes the weight of PAN nanofiber membrane). Considering cost,

time and energy consumption, the insignificant difference in the adsorption capacity of 30%4h-PAN@UiO-66-NH₂ and 30%6h-PAN@UiO-66-NH₂ renders the former selective for further studies. In addition to the enhanced reusability of UiO-66-NH₂ particles of 30%4h-PAN@UiO-66-NH₂, it is noteworthy that the adsorption capacity of 30%4h-PAN@UiO-66-NH₂ was ~15 times better than that of PAN nanofiber membrane.

3.8 Adsorption Kinetics

Adsorption time is a key factor in evaluating the removal rate of adsorbents. Figure 7a shows The Cr(VI) adsorption time on 30%4h-PAN@UiO-66-NH₂ at three different initial concentrations. It is observed that adsorption increases with the prolongation of adsorption time and reaches equilibrium above 300 min. Among them, the adsorption capacity of Cr(VI) on 30%4h-PAN@UiO-66-NH₂ nanofiber membrane rapidly increase within 240 min, which may be assigned to abundant adsorption sites on the surface of 30%4h-PAN@UiO-66-NH₂. Afterward, the adsorption efficiency gradually decreases until almost all 100 mg/g Cr(VI) in the solution was adsorbed. Comparing the three adsorption curves of different Cr(VI) concentrations, it is ascertained that adsorption capacity of 30%4h-PAN@UiO-66-NH₂ increases as the initial Cr(VI) concentration increases from 50 to 100 mg/L. For further clarification, the adsorption mechanism of 30%4h-PAN@UiO-66-NH₂ nanofiber membranes were described using kinetic model, pseudo-first-order model and pseudo-second-order model (as shown in Figs. (b), (c), (d) and (f)). The relevant kinetic data were fitted to obtain the relevant kinetic parameters (Tables 2, 3).

To eliminate modeling bias and identify modeling traps, linear and nonlinear fitting were performed on the pseudo first order dynamics model and pseudo second order dynamics model, respectively, using two different fitting methods [31] (Fig. 7b–d). Comparing the data in Table 2, it was found

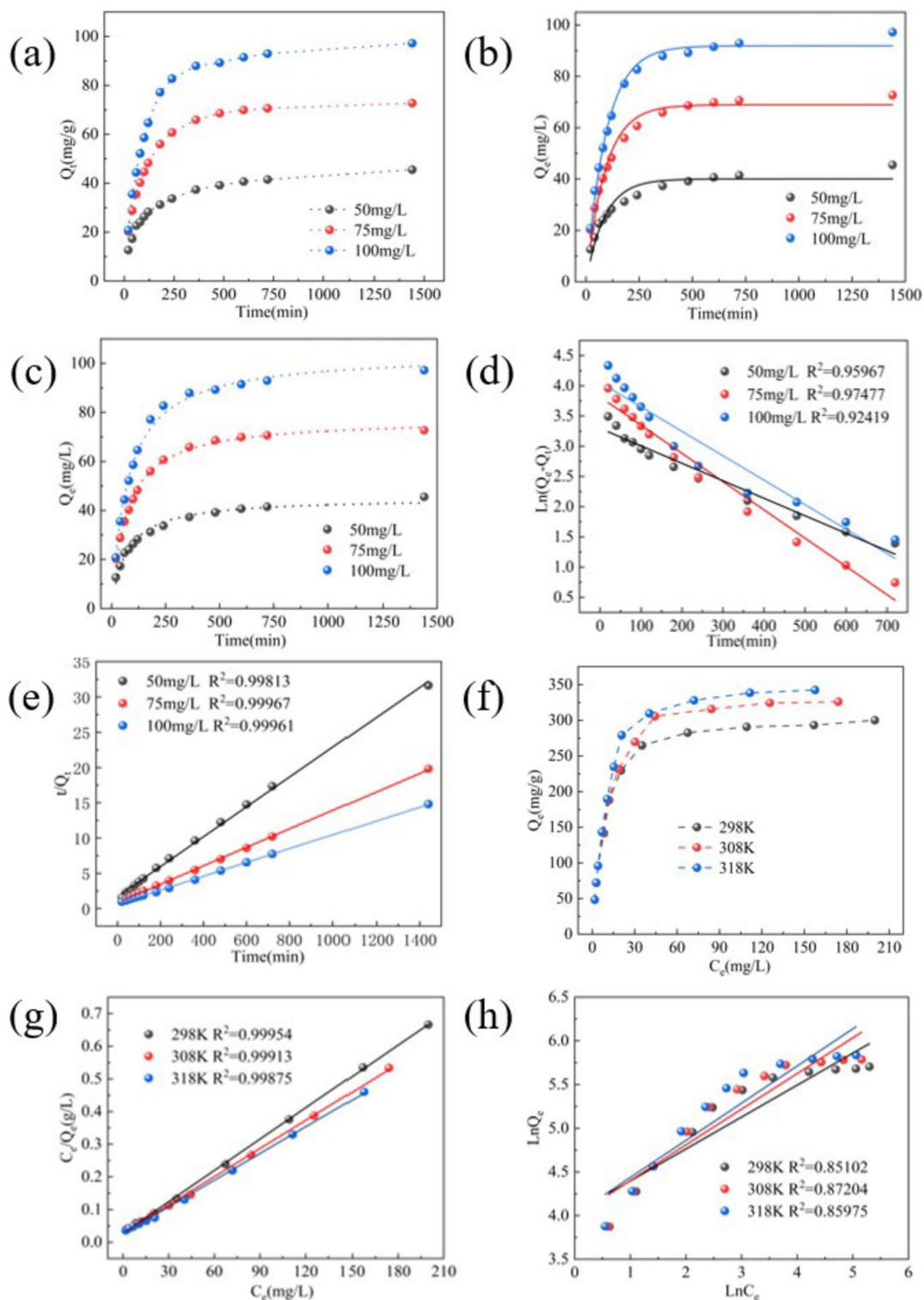


Fig. 7 **a** Adsorption kinetics for Cr(VI) at 50, 75, and 100 mg/L on 30%4h-PAN@UiO-66-NH₂ nanofiber membrane. **b** Nonlinear fitting of pseudo-first-order kinetics. **c** Nonlinear fitting of pseudo-second-order kinetics. **d** Linear fitting of pseudo-first-order kinetics. **e** Lin-

ear fitting of pseudo-second-order kinetics. **f** Adsorption isotherm of Cr(VI) at 298, 308, and 318 K. **g** Langmuir isotherm. **h** Freundlich isotherm on 30%4h-PAN@UiO-66-NH₂ nanofiber membrane

that although the R^2 values of the two are very close, there is a significant difference in their Q_e values. Experimental work reveals that the nonlinear fitting of the pseudo first-order dynamic model was closer to the actual experimental values. Consequently, the nonlinear fitting parameters were selected for subsequent comparison. Similarly, the linear fitting of the pseudo second-order kinetic model is closer to the actual experimental values (as shown in Table 3). Critical comparison reveals that higher correlation coefficients ($R^2 > 0.99$) and close-to-actual experimental values were obtained in pseudo second-order kinetic model. This indicates that 30%4h-PAN@UiO-66-NH₂ nanofiber membrane was more in line with the pseudo-second-order kinetic model. It was further confirmed that the adsorption behavior of 30%4h-PAN@UiO-66-NH₂ nanofiber membrane followed the chemical adsorption mode, which was characterized by strong attraction and fast Cr(VI) removal rate [32].

The effect of initial concentration and temperature on the adsorption of Cr(VI) on 30%4h-PAN@UiO-66-NH₂ nanofibrous membrane is presented in Fig. 7f. The adsorption capacity of the sample increases as the temperature and initial Cr(VI) concentration increase. This implies that there were numerous adsorption sites on surface of 30%4h-PAN@UiO-66-NH₂ which enhanced the adsorption of Cr(VI) until equilibrium was reached. At the same time, under the same

initial concentration, with the increase in temperature, the adsorption capacity increased.

Langmuir isotherm model and the Freundlich isotherm model were explored to describe the interaction in the adsorption process (Fig. 7g, h), and the relevant adsorption isotherm data were fitted to obtain related adsorption isotherm parameters (Table 4). It can be seen that the correlation coefficient (R^2) value of Langmuir model was greater than that of Freundlich model. This implies that Cr(VI) is mainly removed in the form of monolayer adsorption on the surface of 30%4h-PAN@UiO-66-NH₂ nanofiber membrane [10, 14]. The maximum adsorption capacity of Cr(VI) reported by other adsorbents in recent years is shown in Table 5. It can be clearly seen that the maximum adsorption capacity of 30%4h-PAN@UiO-66-NH₂ in this study is 312.25 mg/g, which is higher than other adsorbents in the literature [12, 13, 33–37].

3.9 Influence of Interference Ions on Adsorption

In actual wastewater treatment, there are a large number of other ionic pollutants that actively compete with each other for adsorption sites. Therefore, it is imperative to explore the effect of interfering ions on the adsorption of Cr(VI). Figure 8a shows that in a metal cation solution system,

Table 2 Relevant pseudo-first-order model parameters of 30%4h-PAN@UiO-66-NH₂ nanofiber membrane

Cr(VI) mg/L	Pseudo-first-order model						
	$Q_{e \text{ exp}}$ (mg/L)	Nonlinear fitting model			Linear fitting model		
		K_1 (min ⁻¹)	Q_e (mg/g)	R^2	K_2 (min·g/mg)	Q_e (mg/g)	R^2
50	45.51	0.01138	40.02	0.907	0.00289	27.12	0.960
75	72.70	0.01103	68.89	0.964	0.00468	45.49	0.975
100	97.21	0.01057	91.90	0.989	0.00405	57.36	0.924

Table 3 Relevant pseudo-second-order model parameters of 30%4h-PAN@UiO-66-NH₂ nanofiber membrane

Cr(VI) mg/L	Pseudo-second-order model						
	$Q_{e \text{ exp}}$ (mg/g)	Nonlinear fitting model			Linear fitting model		
		K_1 (min ⁻¹)	Q_e (mg/g)	R^2	K_2 (min·g/mg)	Q_e (mg/g)	R^2
50	45.51	0.00032	45.14	0.982	0.00026	47.24	0.998
75	72.70	0.00019	77.41	0.995	0.00020	76.39	0.999
100	97.21	0.00013	104.1	0.993	0.00014	102.24	0.999

Table 4 Adsorption isotherm parameters of 30%4h-PAN@UiO-66-NH₂ at different temperature

Temperature K	Langmuir model				Freundlich model		
	$Q_{e \text{ exp}}$ (mg/g)	Q_m (mg/g)	K_L (mg/L)	R^2	$1/n$	K_F (L/g)	R^2
298	300.12	312.25	0.115	0.999	0.365	56.316	0.851
308	325.98	348.43	0.102	0.999	0.408	54.192	0.872
318	342.40	367.64	0.103	0.998	0.425	55.181	0.860

Table 5 Adsorption capacity of different adsorbents for Cr(VI) removal

Adsorbent	Q_m (mg/g)	pH	Temperature (K)	References
30%4h-PAN@UiO-66-NH ₂	312.5	2	298	This work
CP	299.89	3	318	[31]
CTS/CS-50	130.41	2	298	[32]
UiO-66 Modified Corncob	90.04	6.5	298	[33]
UiO-66-NH ₂ /MoS ₂ @PUF	125	2	303	[34]
Modified UiO-66-NH ₂ with phenothiazine- <i>N</i> -rhodanine	333.67	2	303	[12]
Formic acid-modified-UiO-66	243.9	2	298	[13]
UiO-66-NH ₂ @silica	277.4	5	Not provided	[35]

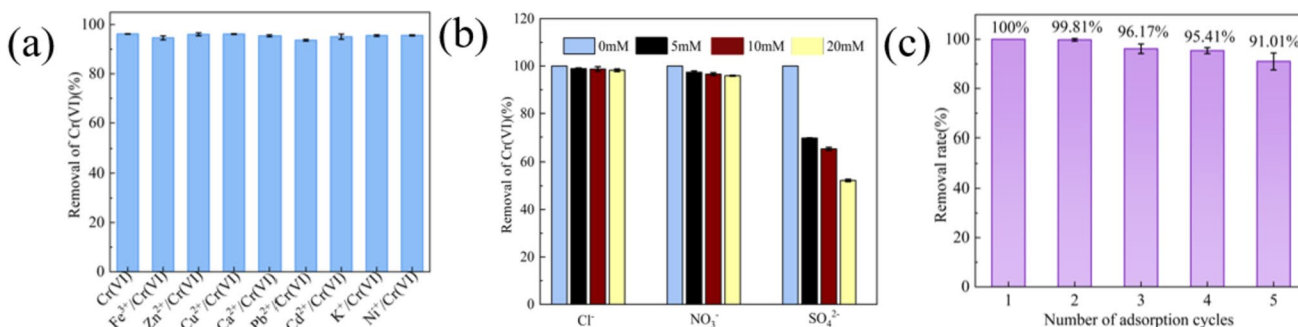


Fig. 8 **a** Effect of coexisting cations on Cr(VI) adsorption by 30%4h-PAN@UiO-66-NH₂ nanofiber membrane. **b** Adsorption capacity of coexisting anions on Cr(VI) by 30%4h-PAN@UiO-66-NH₂ nanofiber

membrane. **c** Cyclic adsorption of Cr(VI) by 30%4h-PAN@UiO-66-NH₂ nanofiber membrane

30%4h-PAN@UiO-66-NH₂ nanofiber membrane exhibits selective adsorption of Cr(VI). Figure 8b shows an insignificant decrease in selective adsorption capacity of Cr(VI) on 30%4h-PAN@UiO-66-NH₂ nanofiber membrane in anionic solution system (for monovalent anions NO₃³⁻ and Cl⁻), regardless the increase in the concentration of coexisting ions. However, when divalent anion SO₄²⁻ was added, the selective adsorption capacity for Cr(VI) significantly decreases. This is due to the large radius of divalent anion SO₄²⁻ which makes the electrostatic adsorption capacity and ion energy of divalent SO₄²⁻ exceed that of monovalent NO₃³⁻ and Cl⁻ ions [38].

3.10 Reusability of Adsorbent

Figure 8c shows the reusability of 30%4h-PAN-UiO-66-NH₂ in five cycles. Generally, the adsorption performance slightly decreased in the 5th cycle compared to the 1st cycle, but still maintained more than 90% removal rate. This indicates that 30%4h-PAN@UiO-66-NH₂ nanofiber membrane has good reusability and easy recyclability. This novelty helps overcome the challenge in recycling of UiO-66-NH₂ particles and avoidance of potential secondary pollution when treating wastewater.

The EDS spectra of 30%4h-PAN@UiO-66-NH₂ before and after adsorption of Cr(VI) is shown in Fig. 9a. At 5.4 keV, a new peak appears, which is assigned to energy spectrum peak of Cr [39], implying adsorption of Cr(VI) on the surface of the adsorbent. Uniformly distributed Cr element on the surface of the 30%4h-PAN@UiO-66-NH₂ nanofiber membrane further proves the successful and even adsorption of chromium on the adsorbent (Fig. 9b).

3.11 Adsorption Mechanism

To propose the adsorption mechanism of 30%4h-PAN@UiO-66-NH₂ nanofiber membrane, the effects of pre- and post-adsorption on 30%4h-PAN@UiO-66-NH₂ nanofiber membrane was examined using XPS. As shown in Fig. 9c, the characteristic peak of Cr on 30%4h-PAN@UiO-66-NH₂-after adsorption indicates that Cr(VI) was successfully adsorbed on the 30%4h-PAN@UiO-66-NH₂. The obvious Cr 2p peak identified on 30%4h-PAN@UiO-66-NH₂ after adsorption was deconvoluted to clearly identify the valence state of Cr(VI) (Fig. 9d). The binding energies at 586.18 and 576.58 eV are assignable to Cr(III), while 588.08 and 578.48 eV are assigned to Cr(VI) [40]. It can be observed that more Cr (III) are present on the surface than Cr(VI). This implies that Cr(VI) is reduced to Cr(III). The peaks

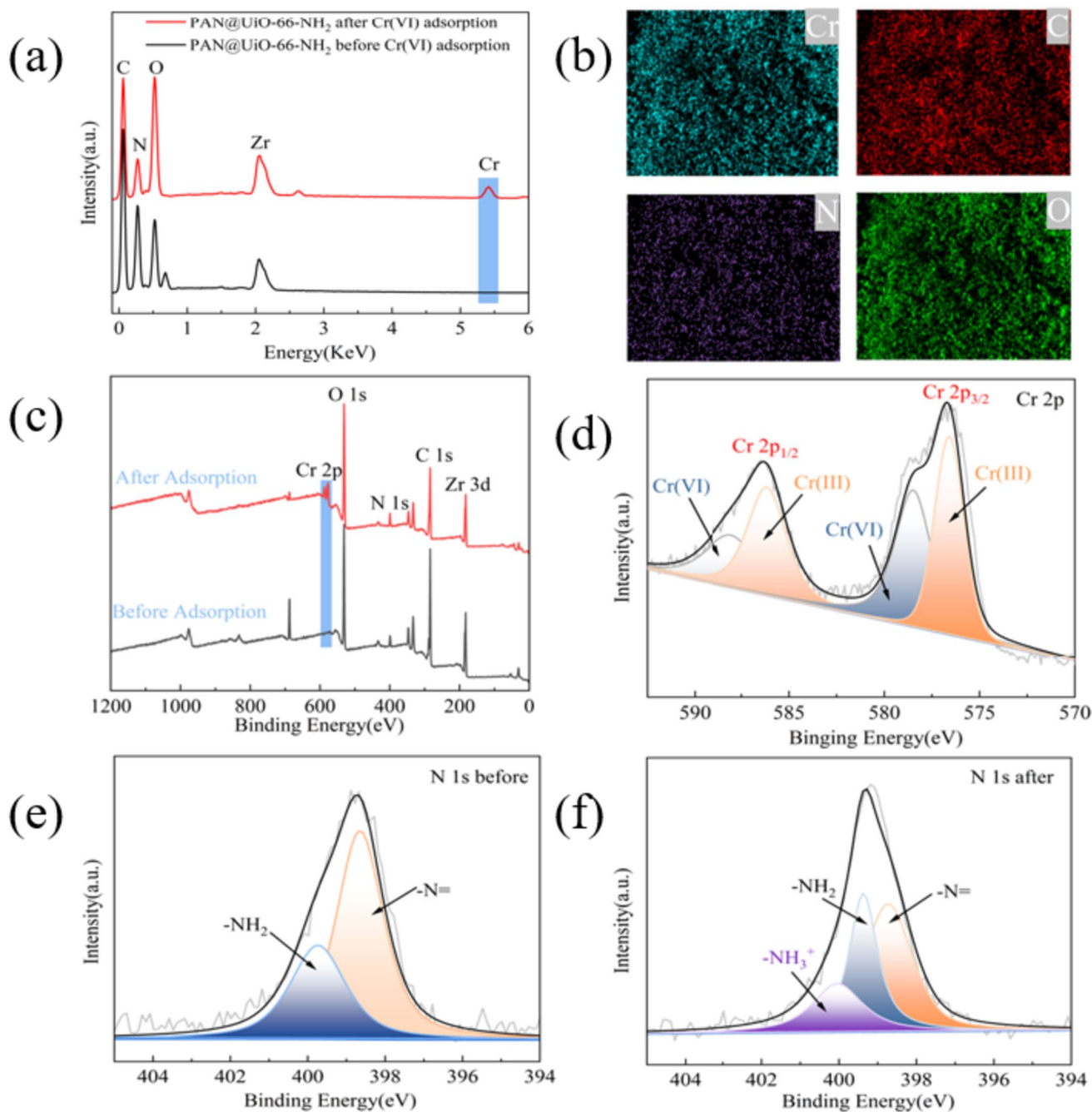


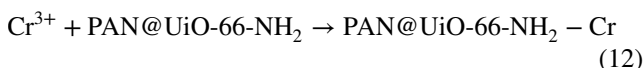
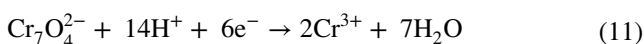
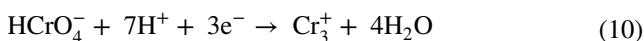
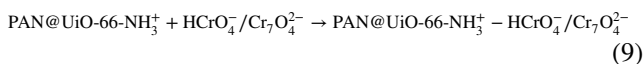
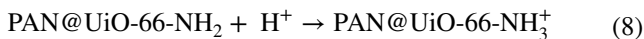
Fig. 9 **a** EDS spectra of 30%4h-PAN@UiO-66-NH₂ nanofiber membrane before and after Cr(VI) adsorption and **b** mapping results of 30%4h-PAN@UiO-66-NH₂ nanofiber membrane after Cr(VI) adsorption. **c** Full XPS spectra of 30%4h-PAN@UiO-66-NH₂ nanofiber membrane before and after Cr(VI) adsorption, **d** Cr2p spectrum of

30%4h-PAN@UiO-66-NH₂ nanofiber membrane after Cr(VI) adsorption. **e** Peak N1s of 30%4h-PAN@UiO-66-NH₂ nanofiber membrane. **f** Peak N1s of 30%4h-PAN@UiO-66-NH₂ nanofiber membrane after Cr(VI) adsorption

centered at 399.78 and 398.68 eV appear in the XPS spectra of N1s correspond to -NH₂ and imine (-N=) functional groups (Fig. 9e, d). There is a new peak at 400.08 eV in the XPS spectrum of N1s after adsorption of Cr(VI) on sample, which belongs to NH₃⁺. This indicates that amine matrix is seeded during adsorption [41].

Based on the XPS results, the proposed mechanism for the adsorption of Cr(VI) on 30%4h-PAN@UiO-66-NH₂ nanofiber membrane is as follows: first, under acidic conditions, the amino group on the 30%4h-PAN@UiO-66-NH₂ nanofiber membrane obtains hydrogen ions which protonates into NH₃⁺, making the surface positively charged, hence

enhancing adsorption of anion Cr(VI) through electrostatic attraction [38]. This step is a key path for removal of Cr(VI) on 30%4h-PAN@UiO-66-NH₂ nanofiber membrane. Secondly, -NH₂ on the 30%4h-PAN@UiO-66-NH₂ nanofiber membrane donates electrons to reduce adsorbed Cr(VI) to Cr(III). The specific reactions are as follows in (8)–(12). Finally, the reduced Cr(III) can be adsorbed on the surface of the nanofiber membrane by forming a chelate with -NH₂.



4 Conclusion

In this paper, PAN@UiO-66-NH₂ nanofiber membrane was developed using water as solvent and trifluoroacetic acid as regulator and applied as adsorbent for the removal of Cr(VI). Based on FT-IR, XRD, TG, EDS, BET results and adsorption test, 30% trifluoroacetic acid concentration, 4 h hydrothermal synthesis time and pH = 2 were identified as the suitable conditions for the successful synthesis of large surface area PAN@UiO-66-NH₂ with good adsorption performance. According to the analysis of adsorption kinetics and adsorption isotherm, 30%4h-PAN@UiO-66-NH₂ nanofiber membrane is more in line with the pseudo-second-order adsorption kinetic model and the Langmuir model, and its adsorption process follows the chemical adsorption mode. It recorded excellent adsorption performance, with maximum adsorption capacity of 312.25 mg/g. Generally, the interference cations and anions had insignificant influence on the selective adsorption of Cr(VI) on 30%4h-PAN@UiO-66-NH₂. Aside the good performance, the 30%4h-PAN@UiO-66-NH₂ nanofiber membrane exhibits better reusability, recording more than 90% Cr(VI) adsorption rate after five cycles. XPS analysis shows that the adsorption mechanism of Cr(VI) on 30%4h-PAN@UiO-66-NH₂ nanofiber membrane is mainly through electrostatic attraction, in which the adsorbed Cr(VI) is reduced to Cr(III), and finally chelated material form is absorbed. Conclusively, the as-prepared 30%4h-PAN@UiO-66-NH₂ nanofiber membrane is an

effective adsorbent for the removal of Cr(VI) in industrial wastewater.

Acknowledgements This work was supported by Anhui Provincial Natural Science Foundation General Project (2008085ME139); Anhui Province Key R&D and Development Plan Project (2022107020006).

Data Availability Data will be made available on request.

Declarations

Conflict of interest All authors have declared no conflict of interest.

References

1. Q. Feng, D.S. Wu, Y. Zhao, A.F. Wei, H. Fong, Electrospun AOPAN/RC blend nanofiber membrane for efficient removal of heavy metal ions from water. *J. Hazard. Mater.* **344**, 819–828 (2018)
2. Y.Y. Huang, H.L. Zheng, X.B. Hu, Y.Y. Wu, X.H. Tang, Q. He, S.Y. Peng, Enhanced selective adsorption of lead(II) from complex wastewater by DTPA functionalized chitosan-coated magnetic silica nanoparticles based on anion-synergism. *J. Hazard. Mater.* **422**, 126856 (2021)
3. H.T. Zeng, H.H. Zeng, H. Zhang, A. Shahab, K. Zhang, Y.Q. Lu, L. Nabi, F.Z. Naseem, H. Ullah, Efficient adsorption of Cr(VI) from aqueous environments by phosphoric acid activated eucalyptus biochar. *Clean Prod.* **286**, 124964 (2020)
4. A.K. Verma, R.R. Dash, P. Bhunia, A review on chemical coagulation/flocculation technologies for removal of color from textile wastewaters. *J. Environ. Manag.* **93**(1), 154–168 (2012)
5. Z.Z. Su, B.X. Zhang, J.L. Zhang, X.Y. Cheng, F.Y. Zhang, Q. Wan, L.F. Liu, X.N. Tan, D.X. Tan, L.R. Zheng, J.L. Zhang, Ultra-small UiO-66-NH₂ nanoparticles immobilized on g-C₃N₄ nanosheets for enhanced catalytic activity. *Green Energy Environ.* **7**(3), 512–518 (2022)
6. M. Guo, S.Y. Dong, J. Xiong, X.Y. Jin, P.F. Wan, S.J. Lu, Y.F. Zhang, J. Xu, H.S. Fan, Flexible core-shell PAN/CNTs@PVDF-HFP/UiO-66-NH₂ hybrid nanofibers membrane for advanced lithium-ion batteries separator. *Mater. Today Chem.* **30**, 101552 (2023)
7. J.J. Pan, L.J. Wang, Y.X. Shi, L.L. Li, Z. Xu, H. Sun, F. Guo, W.L. Shi, Construction of nanodiamonds/UiO-66-NH₂ heterojunction for boosted visible-light photocatalytic degradation of antibiotics. *Sep. Purif. Technol.* **284**, 120270 (2022)
8. Y.J. Cui, B. Li, H.J. He, W. Zhou, B.L. Chen, G.D. Qian, Metal-organic frameworks as platforms for functional materials. *Acc. Chem. Res.* **49**(3), 483–493 (2016)
9. X.L. Liu, Metal-organic framework UiO-66 membranes. *Front. Chem. Sci. Eng.* **14**(2), 216–232 (2020)
10. S.B. Wu, Y.J. Ge, Y.Q. Wang, X. Chen, F.F. Li, X. Han, Adsorption of Cr(VI) on nano UiO-66-NH₂ MOFs in water. *Environ. Technol.* **39**(15), 1937–1948 (2018)
11. I. Stassen, J.H. Dou, C. Hendon, M. Dinca, Chemiresistive sensing of ambient CO₂ by an autogenously hydrated Cu₃(hexaiminobenzene)₂ framework. *ACS Cent. Sci.* **5**(8), 1425–1431 (2019)
12. H. Wang, S. Wang, S.X. Wang, L.B. Zhang, Y. Zhou, F. Yang, Efficient and selective removal of Cr(VI) by the modified UiO-66-NH₂ with phenothiazine-*N*-rhodanine from aqueous solution: performance and mechanisms. *Micropor. Mesopor. Mater.* **336**, 111834 (2022)

13. Y.L. Wang, N. Zhang, D.N. Chan, D. Ma, G.G. Liu, X.G. Zou, Y.P. Chen, R.J. Shu, Q.Y. Song, W.Y. Lv, Facile synthesis of acid-modified UiO-66 to enhance the removal of Cr(VI) from aqueous solutions. *Sci. Total. Environ.* **682**, 118–127 (2019)
14. X.L. Zhang, Y.X. Sun, Y.F. Liu, Z.Y. Zhai, S.Q. Guo, L.C. Peng, Y. Qin, C.J. Li, UiO-66-NH₂ fabrics: role of Trifluoroacetic acid as a modulator on MOF uniform coating on electrospun nanofibers and efficient decontamination of chemical warfare agent simulants. *Appl. Mater. Interfaces* **13**, 39976–39984 (2021)
15. S. Jamshidifarda, S. Koushkbagh, S. Hosseini, S. Rezaei, A. Karamipoure, A. Jafarirad, M. Iranig, Incorporation of UiO-66-NH₂ MOF into the PAN/chitosan nanofibers for adsorption and membrane filtration of Pb(II), Cd(II) and Cr(VI) ions from aqueous solutions. *J. Hazard. Mater.* **368**, 10–20 (2019)
16. L. Zhang, H. Chen, X. Bai, S. Wang, L.L. Li, L. Shao, W.X. He, Y.N. Li, T.Q. Wang, X.M. Zhang, J.Y. Chen, Y. Fu, Fabrication of 2D metal-organic framework nanosheet@fiber composites by spray technique. *Chem. Commun.* **55**(57), 8293 (2019)
17. H.Z. Rada, R.H. Abid, H.Q. Sun, J. Shang, J.Y. Lie, Y.D. He, S.M. Liu, S.B. Wang, Effects of –NO₂ and –NH₂ functional groups in mixed-linker Zr-based MOFs on gas adsorption of CO₂ and CH₄. *Prog. Nat. Sci.-Mater.* **28**(02), 160–167 (2018)
18. S.B. Wang, Y. Lin, J. Yang, L. Shi, G. Yang, X.P. Zhuang, Z.H. Li, UiO-66-NH₂ functionalized cellulose nanofibers embedded in sulfonated polysulfone as proton exchange membrane. *Int. J. Hydrogen Energy* **44**(36), 106–115 (2021)
19. F. Ahmadijokani, S. Ahmadipouya, M.H. Haris, M. Rezakazemi, A. Bokhari, H. Molavi, M. Ahmadipour, S.Y. Pung, J.J. Klemeš, T.M. Aminabhavi, M. Arjmand, Magnetic nitrogen-rich UiO-66 metal–organic framework: an efficient adsorbent for water treatment. *Appl. Mater. Interfaces* **15**, 30106–30116 (2023)
20. Y.A.Y.A. Mohammed, A.M. Abdel-Mohsen, Q.J. Zhang, M. Younas, L.B. Zhong, J.C.E. Yang, Y.M. Zheng, Facile synthesis of ZIF-8 incorporated electrospun PAN/PEI nanofibrous composite membrane for efficient Cr(VI) adsorption from water. *Chem. Eng. J.* **461**, 141972 (2023)
21. K.K. Ma, T. Islamoglu, Z. Chen, Z.J. Chen, P. Li, M.C. Wasson, Y.W. Chen, Y.F. Wang, G.W. Peterson, J.H. Xin, O.K. Farha, Scalable and template-free aqueous synthesis of zirconium-based metal–organic framework coating on textile fiber. *JCAS* **141**(39), 15626–15633 (2019)
22. F. Yu, L.S. Cen, C.H. Lei, F.C. Zhu, L. Zhou, H.L. Zhu, B. Yu, Fabrication of recyclable UiO-66-NH₂/PVDF hybrid fibrous membrane for Cr(VI) removal in wastewater. *J. Ind. Eng. Chem.* **123**, 104–115 (2023)
23. A.S. Shamsabadi, M. Ranjbar, H. Tavanai, Electrospinning of gold nanoparticles incorporated PAN nanofibers via in-situ laser ablation of gold in electrospinning solution. *Mater. Res. Express* **6**, 055051 (2019)
24. R. Soltani, R. Pelalak, M. Pishnamazi, A. Marjani, S.M. Sarkar, A.B. Albadarin, S. Shirazian, Novel bimodal micro-mesoporous Ni₅₀Co₅₀-LDH/UiO-66-NH₂ nanocomposite for Tl(I) adsorption. *Arab. J. Chem.* **14**(4), 103058 (2021)
25. L.P. Wang, X.R. Dai, Z. Man, X.R. Li, Y.F. Jiang, D.Z. Liu, H. Xiao, S.J. Sha, Dynamics and treatability of heavy metals in pig farm effluent wastewater by using UiO-66 and UiO-66-NH₂ nanomaterials as adsorbents. *Water Air Soil Pollut.* **232**(7), 294 (2021)
26. X.F. Zhang, Z.G. Wang, J.F. Yao, Y. Feng, Y.X. Zhong, J.Q. Liao, Y.G. Wang, Adsorptive desulfurization from the model fuels by functionalized UiO-66(Zr). *Fuel* **234**, 256–262 (2018)
27. R. Xu, T. Wu, C. Li, X.L. Jiao, D.R. Chen, Self-assembled MOF-on-MOF nanofabrics for synergistic detoxification of chemical warfare agent simulants. *Appl. Mater. Interfaces* **15**, 30360–30371 (2023)
28. X.K. Hao, Z.Y. Zhai, Y.X. Sun, C.J. Li, Preparation and performance characterization of flexible and washable Zr-MOFs composite nanofiber membrane. *Acta Chim. Sinica* **80**(1), 49–55 (2022)
29. K. Pattarith, D. Nugroho, S. Nanan, R. Benchawattananon, Cellulose modified with polyethylenimine (PEI) using microwave methodology for adsorption of chromium from aqueous solutions. *Molecules* **28**, 4514 (2023)
30. Z.Y. Kang, H. Gao, X.L. Ma, X.D. Jia, D.S. Wen, Fe–Ni/MWCNTs nano-composites for hexavalent chromium reduction in aqueous environment. *Molecules* **28**, 4412 (2023)
31. E.D. Revellame, D.L. Fortela, W. Sharp, R. Hernandez, M.E. Zappi, Adsorption kinetic modeling using pseudo-first order and pseudo-second order rate laws: a review. *Clean. Eng. Technol.* **1**, 100032 (2020)
32. M. Jurcic, W.J. Peveler, C.N. Savory, D.K. Bucar, A.J. Kenyon, D.O. Scanlon, I.P. Parkin, Sensing and discrimination of explosives at variable concentration with a large-pore MOF as part of a luminescent array. *Appl. Mater. Interfaces* **501**(12), 518–524 (2019)
33. S.Q. Han, X.L. Zhou, H.H. Xie, X.H. Wang, L.Z. Yang, H.L. Wang, C. Hao, Chitosan-based composite microspheres for treatment of hexavalent chromium and EBBR from aqueous solution. *Chemosphere* **305**, 135486 (2022)
34. S.J. Wu, M.Y. Li, L.L. Xin, H.M. Long, X.P. Gao, Efficient removal of Cr(VI) by triethylenetetramine modified sodium alginate/carbonized chitosan composite via adsorption and photocatalytic reduction. *J. Mol. Liq.* **366**, 120160 (2022)
35. H.Z. Xie, L.W. Yan, H. Chen, C.G. Xiong, L.Q. Wang, Q. Xu, X. Li, Q.H. Zhou, Cr(VI) adsorption from aqueous solution by UiO-66 modified corncob. *Sustainability* **13**(23), 685969 (2021)
36. L.F. Ren, X.D. Gao, X.Y. Zhang, T.T. Qiang, Preparation and adsorption performance of UiO-66-NH₂/MoS₂@PUF for Cr(VI). *Fine Chem.* **40**(02), 398–406 (2023)
37. W.A. El-Mehalmey, A.H. Ibrahim, A.A. Abugable, M.H. Hassan, R.R. Haikal, S.G. Karakalos, O. Zaki, M.H. Alkordi, Metal–organic framework@silica as a stationary phase sorbent for rapid and cost-effective removal of hexavalent chromium. *J. Mater. Chem. A* **10**, 1039 (2018)
38. Y.R. Peng, M. Azeem, R.H. Li, L.B. Xing, Y.M. Li, Y.C. Zhang, Z.Q. Guo, Q. Wang, H.H. Ngo, G.Z. Qu, Z.Q. Zhang, Zirconium hydroxide nanoparticle encapsulated magnetic biochar composite derived from rice residue: application for As(III) and As(V) polluted water purification. *J. Hazard. Mater.* **423**, 127081 (2022)
39. X.H. Wang, X. Li, L.L. Peng, S.Q. Han, C. Hao, C.L. Jiang, H.L. Wang, X.B. Fan, Effective removal of heavy metals from water using porous lignin-based adsorbents. *Chemosphere* **279**, 130504 (2021)
40. X.P. Gao, C. Guo, J.J. Hao, Y. Zhang, M.Y. Li, Z. Zhao, Efficient removal of Cr(VI) by modified sodium alginate via synergistic adsorption and photocatalytic reduction. *Appl. Surf. Sci.* **579**, 152259 (2022)
41. S.Y. Bao, W.W. Yang, Y.J. Wang, Y.S. Yua, Y.Y. Sun, K.F. Li, PEI grafted amino-functionalized graphene oxide nanosheets for ultrafast and high selectivity removal of Cr(VI) from aqueous solutions by adsorption combined with reduction: behaviors and mechanisms. *Chem. Eng. J.* **399**, 125762 (2020)

Springer Nature or its licensor (e.g. a society or other partner) holds exclusive rights to this article under a publishing agreement with the author(s) or other rightsholder(s); author self-archiving of the accepted manuscript version of this article is solely governed by the terms of such publishing agreement and applicable law.